BIOCHEMISTRY

Identifying a next-generation antimalarial trioxolane in a landscape of artemisinin partial resistance

Matthew T. Klope[1]†, Poulami Talukder[1]†, Brian R. Blank[1], Sevil Chelebieva[2], Jun Chen[1], Shaun D. Fontaine[3], Ryan L. Gonciarz[1], Priyadarshini Jaishankar[1], Grace J. Lee[3], Jennifer Legac[4], Vineet Mathur[1], Avani Narayan[1], Martin Okitwi[4], Stephen Orena[4], Nicholas S. Settineri[5], Juan A. Tapia[1,6], Yoweri Taremwa[4], Patrick K. Tumwebaze[4], Aswathy Vinod[1], Jeremy N. Burrows[7], Philip J. Rosenthal[6], Roland A. Cooper[2]‡, Adam R. Renslo[1]*

For over two decades, artemisinin-based combination therapy (ACT) has been the standard of care for the treatment of uncomplicated falciparum malaria. However, artemisinin partial resistance (ART-R) is now prevalent in Southeast Asia and has emerged in eastern Africa, threatening ACT efficacy. Artefenomel, a synthetic 1,2,4-trioxolane, exhibits an extended pharmacokinetic exposure profile that predicts for efficacy against ART-R parasites. Unfortunately, the development of artefenomel was halted recently after almost a decade in the clinic. Here, we describe studies of an artefenomel-adjacent chemotype that combines potent in vitro activity against clinical ART-R parasites, an extended pharmacokinetic profile with single-exposure efficacy in a murine malaria model, and enhanced stability in human microsomes and hepatocytes. Overall, our studies reveal a heretofore underexplored trioxolane chemotype with the potential to address ART-R in a next-generation trioxolane development candidate.

INTRODUCTION

For two decades, artemisinin-based combination therapy (ACT) has been the standard of care to treat uncomplicated falciparum malaria, likely saving millions of lives (*1*). The unusual molecular pharmacology of artemisinins involves chemical activation by free ferrous heme in the parasite (*2*–*4*), promiscuous covalent modification of parasite proteins (*5*–*7*), and potent killing of all asexual erythrocytic stages of the etiological agent, *Plasmodium falciparum* (*8*). Inspired by these agents and their clinical utility, researchers have long sought to identify synthetic endoperoxides whose pharmacokinetic (PK) properties could be more readily optimized to overcome the rapid clearance profile of dihydroartemisinin (DHA), the common active metabolite of all clinically used artemisinins (Fig. 1). Among various chemotypes explored (*9*), only the 1,2,4-trioxolanes arterolane (*10*) and artefenomel (**1**; Fig. 1) have advanced to clinical trials (*11*, *12*). While arterolane is approved in India and some African countries as a combination with piperaquine, its PK profile is only marginally improved over that of DHA, and the drug has seen limited clinical use. Higher hopes were invested in artefenomel, which combines an extended in vivo exposure profile and produces single-exposure cures in preclinical models, an important (*13*, *14*) benchmark in antimalarial discovery. Whether single-exposure cure is a reasonable clinical benchmark remains controversial (*15*), and the clinical development of **1** was recently discontinued after more than a decade of studies aiming to achieve single-exposure cures in patients with malaria (*16*–*18*).

[1]Department of Pharmaceutical Chemistry, University of California, San Francisco, San Francisco, CA, USA. [2]Dominican University of California, San Rafael, CA, USA. [3]Departments of Chemistry and In Vivo Pharmacology, Tatara Therapeutics, San Francisco, CA, USA. [4]Infectious Diseases Research Collaboration, Kampala, Uganda. [5]Advanced Light Source, Lawrence Berkeley National Laboratory and Department of Chemistry, University of California, Berkeley, Berkeley, CA 94720, USA. [6]Department of Medicine, San Francisco General Hospital, University of California, San Francisco, San Francisco, CA, USA. [7]Medicines for Malaria Venture, International Center Cointrin, Route de Pré-Bois 20, 1215 Geneva, Switzerland.
*Corresponding author. Email: adam.renslo@ucsf.edu
†These authors contributed equally to this work.
‡Deceased.

Given the central role of artemisinins in ACT, the emergence of artemisinin partial resistance (ART-R) in Southeast Asia (*19*) and its more recent emergence in eastern Africa (*20*, *21*) is of considerable concern (*22*). Clinically, the ART-R phenotype manifests as delayed parasite clearance that can be accompanied by treatment failures, in particular with coexistent resistance to ACT partner drugs. Mechanistically, ART-R is associated with destabilizing mutations (*19*, *23*) in the propeller domain of the *Kelch13* (K13) protein, causing an endocytosis defect that reduces parasite uptake of host hemoglobin, thus limiting the parasite pool of artemisinin-activating free heme iron, particularly in early rings (*24*, *25*). This mechanism is supported by recent studies defining the role of the K13 protein in parasite endocytosis (*24*, *26*) and by earlier studies in which an ART-R phenotype was observed in parasites deficient in hemoglobin catabolism (*27*, *28*). In summary, the relative resistance of K13 mutant rings to DHA, combined with the drug's rapid in vivo clearance profile, allows K13 mutant *P. falciparum* to survive brief DHA exposure and progress through the erythrocytic cycle.

The unusual, ring stage–specific resistance of K13 mutant parasites presents interesting challenges and opportunities for the discovery of a next-generation agent. Among the challenges is that traditional in vitro growth inhibition assays do not reveal the reduced susceptibility of ART-R parasites to DHA. To discern the ART-R phenotype in vitro, a ring-stage survival assay (RSA) was developed, in which synchronized ring-stage parasites are subjected to a short pulse of DHA to mimic its PK profile (*29*). Although the assay was explicitly developed to assess susceptibility of parasites to DHA, similar pulsed-exposure experiments have been used to model the PK exposure of **1**, suggesting that this longer-acting agent should be effective clinically against ART-R parasites (*30*, *31*). While this prediction was not wholly borne out in clinical studies with **1** (*18*), the suboptimal dosing paradigm used (i.e., oral suspension) and high rates of emesis suggest that target exposure levels of **1** and partner drug were not achieved, quite possibly leaving this key hypothesis untested.

With an understanding of the molecular mechanism underlying ART-R, it is now possible to take a more rational approach to the

design of next-generation endoperoxide agents. On the one hand, the fact that K13 mutant rings have a limiting pool of activating ferrous iron could argue for an agent with greater iron reactivity. However, such an approach would run counter to the need for good drug stability in the bloodstream of infected patients (*11*) and is further argued against by the reduced stability of endoperoxides at high levels of parasitemia (*32*). We reasoned that a trioxolane agent with enhanced stability toward iron and having an extended exposure profile might persist through the prolonged ring stages of ART-R parasites to realize killing of the more susceptible trophozoite and schizont stages. This activity would depend, of course, on the molecule retaining sufficient iron reactivity (*33*, *34*) to produce the carbon-centered radical species (fig. S1) that confer toxic effects in the parasite (*5*–*7*, *35*). To this end, it is well known (*36*) that the iron sensitivity of the dispiro-1,2,4-trioxolane pharmacophore (as found in **1**) is modulated by conformational dynamics of the cyclohexane ring, which, in turn, are determined by the nature and stereochemistry of the 4″ side chain. Specifically, 1,3-diaxial interactions of the cis-4″ substituent favor a ground-state conformer in which the peroxide bond is shielded by four neighboring axial C─H bonds and prevented from inner-sphere coordination with iron (Fig. 2 and fig. S2). Thus, by using a bulky 4″ aryl side chain, Vennerstrom and colleagues achieved enhanced stability of the endoperoxide function in **1**, while retaining sufficient iron reactivity to exert potent antiparasitic effects (*11*, *37*). To better modulate iron reactivity of the dispiro-1,2,4-trioxolane pharmacophore, our laboratory has explored (*38*–*41*) analogs bearing trans-3″ substitution, based on conformational analyses (Fig. 2 and fig. S2) that suggested a similar degree of stabilization degree as canonical cis-4″ substitution. We found that trans-3″ congeners of arterolane and **1** exhibited potent antiplasmodial activity, both in vitro and in vivo, retaining iron reactivity in a pharmacologically relevant regime (*39*, *41*). Described herein are the results of a systematic exploration of trans-3″ aryl substitution, including extensive in vitro and in vivo characterization of **2** (Fig. 1) as an exemplar of this chemotype that promises to deliver development candidates with differentiated properties, including activity against ART-R parasites.

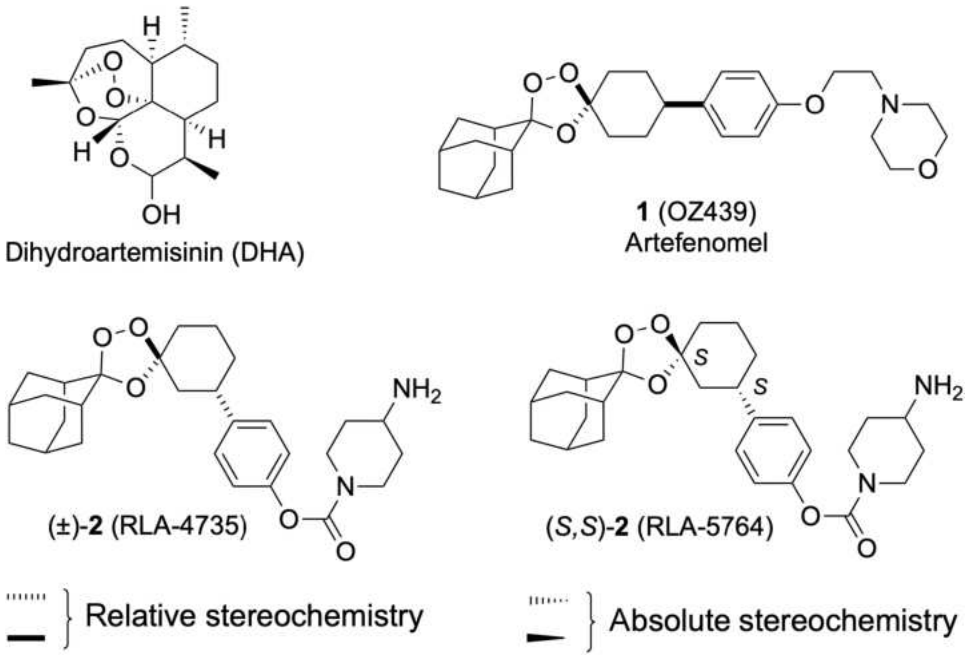

Fig. 1. Structures of DHA, the active metabolite of all clinically used artemisinins, the cis-4″ trioxolane artefenomel (1), and trans-3″ trioxolane analogs (±)-2 and (*S*,*S*)-2. Drawing conventions denoting the relative or absolute configurations of stereocenters are indicated.

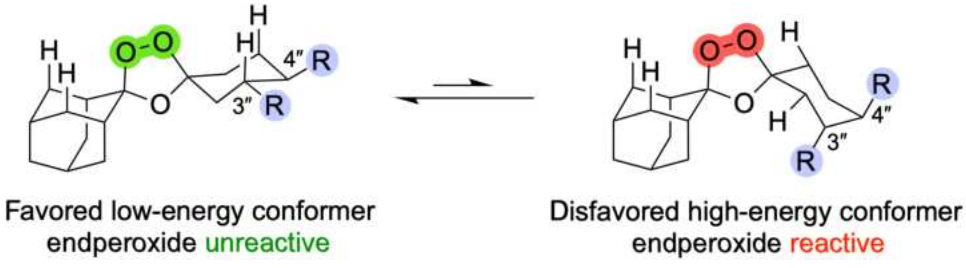

Fig. 2. Iron reactivity of trioxolane antimalarials is determined by conformational equilibria of the cyclohexane ring. Cis-4″ substitution as in **1** or trans-3″ substitution as in **2** and related analogs discussed herein stabilize the endoperoxide bridge (in green and red highlights) in a pharmacologically optimal range for antimalarial effects.

RESULTS

Medicines for Malaria Venture (MMV) has detailed (*14*, *42*) drug product profiles for agents to be used in future antimalarial combination therapies, including Target Candidate Profile 1 (TCP-1), for the rapid reduction of parasite burden in blood stage infections. At the outset of our effort, **1** remained the best hope for a TCP-1 candidate to replace artemisinin, and, thus, **1** was a benchmark compound for our in vitro and in vivo studies. Compound evaluation and progression were guided by three primary assays: (i) in vitro activity against the chloroquine-resistant W2 strain of *P. falciparum*, (ii) in vitro human liver microsome (HLM) apparent intrinsic clearance, and (iii) aqueous solubility in phosphate-buffered saline (PBS) at pH 7.4, the latter two criteria representing the greatest opportunity for improvement over **1**. We also used the *Plasmodium berghei* mouse malaria model to rapidly assess PK/pharmacodynamic (PD) profiles of lead compounds, while recognizing the inherent drawback of this model (e.g., use of a mouse rather than human parasite). Despite this limitation, we expected that analogs having a favorable profile in the three primary assays, and also with strong efficacy in the *P. berghei* model, would prove effective in the context of ART-R, as suggested by previous time-kill studies of **1** and related trioxolane drug candidates (*30*, *31*). As detailed later, advanced leads with this desirable absorption, distribution, metabolism, and excretion (ADME)/PK/PD profile (namely, **2**) showed broad activity against artemisinin susceptible and ART-R, K13 mutant parasites in ex vivo RSA studies of patient samples from 2019 and 2023 to 2024 in Uganda.

Chemically, the change from 4″ to 3″ substitution of the trioxolane pharmacophore results in four possible stereoisomers (versus only two, cis and trans, isomers for 4″ analogs). However, the Griesbaum co-ozonolysis reaction used to prepare the trioxolane ring is an inherently stereoselective process, favoring cis (relative) stereochemistry in the case of 4″-substitution (*43*) and trans stereochemistry in the case of 3″ substitution (*38*). Thus, a four- to six-step synthesis (fig. S3) was sufficient to prepare racemic 3″ analogs such as (±)-**2** and (±)-**3**, the latter (Fig. 3) first described in our initial report on 3″ aryl substitution (*41*). Preparing enantiopure forms of these analogs [i.e., (*R*,*R*)-**2** and (*S*,*S*)-**2**] simply entailed the use of enantiopure cyclohexanone starting material in the Griesbaum reaction (figs. S4 and S5, respectively). A more detailed discussion of the synthesis of trans-3″-aryl trioxolane analogs is provided in the Supplementary Materials.

In our initial report on this chemotype (*41*), we found (±)-**3** to have substantially improved HLM stability and improved solubility in aqueous and polar aprotic solvents such as dimethyl sulfoxide (DMSO), as compared to **1**. The compound retained a PD effect in vivo, producing cures in the *P. berghei* mouse model after a single oral dose of 80 mg/kg. Following on these auspicious findings, we next evaluated the closely related analogs (±)-**4** and (±)-**5**, in which the morpholino side chain is located at the meta or ortho position of the aryl ring, respectively (Fig. 3A and figs. S6 to S8). While meta isomer **4** exhibited in vitro potency similar to that of **3** (~4-fold weaker than **1**), the corresponding ortho isomer **5** was less potent (Table 1). The HLM stability of **4** was comparable to that of **1** (both **4** and **1** inferior to **3**), whereas **5** was rapidly metabolized by HLMs (Table 1). The in vivo efficacy of **3** to **5** following a single dose of 20 mg/kg paralleled their HLM stabilities, with compound **3** affording a greater survival benefit than **4** and compound **5** showing no benefit over vehicle (Fig. 3B). This result appeared to validate our decision to assess human and not mouse liver microsome stabilities during compound optimization and prioritization. Consistent with its well-known efficacy against the *P. berghei* parasite in mice, the artefenomel control was fully curative with just a single dose of 20 mg/kg (*11*).

Next, we systematically explored alteration of the trans-3″ side chains, with a focus on the meta and para substitution pattern (see Supplementary Text for a fuller discussion of structure-activity relationship studies). Briefly, we found that 3″-aryl analogs bearing carbamate side chains terminating in cyclic or acyclic amines had in vitro potencies superior to the ethers **3** to **5** (Fig. 3C and fig. S10). Notably, metabolic trends in the HLM assay mirrored those observed for ethers **3** to **5**, with meta- and para-substituted carbamates generally more stable than ortho congeners. The most promising carbamate analogs such as **2, 9**, **10**, **18**, and **21** (Fig. 3C and fig. S10) combined W2 median inhibitory concentration (IC_{50}) values in the single-digit nanomolar range, with favorable aqueous solubility (mid-micromolar range), and assay-bottoming HLM clearance values of <11 μl/min per milligram, as compared to 72.1 μl/min per milligram for **1** (Table 1 and fig. S10). Thus, these analogs were predicted by initial in vitro measures to be superior to **1** in their drug-like properties. In the *P. berghei* model, an oral dose (20 mg/kg) of meta analogs **9**, **10**, **11**, and **16** produced a median survival of between 9 and 12 days (Fig. 3D), similar but not improved over compound **3** in this model (*41*). Overall, a more promising in vitro profile was noted for para-substituted analogs such as **2**, **18**, and **21** (fig. S10). We thus selected compound **2** for more extensive PK/PD profiling as an exemplar of the seemingly most promising trans-3″ para-carbamate chemotype.

First, we compared the in vivo efficacy and mouse PK of compounds **1** and (±)-**2** and (*R*,*R*)-**6**, a nonaryl, trans-3″ carbamate bearing the same amino terminal side chain of **2** (*40*). We explored single and two-dose regimens of **2** and **6**, selecting either a single dose of 50 mg/kg or two daily doses of 10 mg/kg. Whereas compound **2** produced four of five cures with the single dose of 50 mg/kg and no cures with the two smaller doses, (*R*,*R*)-**6** conversely produced three of five cures with two doses of 10 mg/kg but no cures following the single large dose (Fig. 3E). This result suggested a distinct PK/PD profile for the two chemotypes, confirmed in a mouse PK experiment, with an oral dose (50 mg/kg) of **2** resulting in plasma concentrations above in vitro IC_{50} values for at least 24 hours (Fig. 3F and table S1). By contrast, (*R*,*R*)-**6** was undetectable at 24 hours following a dose of 50 mg/kg, with an area under the curve (AUC) of only ~20% that of **2** and ~6% that of **1** (table S1). Thus, in comparing aryl and nonaryl trans-3″ analogs bearing identical 4-aminopiperidine–terminated side chains, we identified a potential PK/PD advantages of 3-aryl carbamates such as **2**. The enhanced iron stability of **2** versus **6**, as detailed later, may also contribute to a prolonged exposure profile, particularly in infected animals.

Overall, the single-exposure efficacy, superior HLM stability, and improved solubility of analogs like (±)-**2** and (±)-**3** suggested a potential for improved human PK and less complex solution-phase behavior as compared to **1** (*44*, *45*). We next sought to evaluate the in vitro and in vivo properties of enantiomerically pure forms (*R*,*R*)-**2** and (*S*,*S*)-**2**. A small-molecule crystal structure of the form (*R*,*R*)-**2**·HCl (Fig. 4A) confirmed the absolute stereochemistry of the material and validated our asymmetric routes to the enantiopure forms (figs. S4 and S5). In laboratory-adapted clinical strains of *P. falciparum* bearing K13 mutations, both enantiomeric forms of **2** showed potent, low single-digit nanomolar or high picomolar IC_{50} values (Table 2), revealing their intrinsic potency against ART-R parasites. This would later be confirmed in the more informative ex vivo RSA assay of

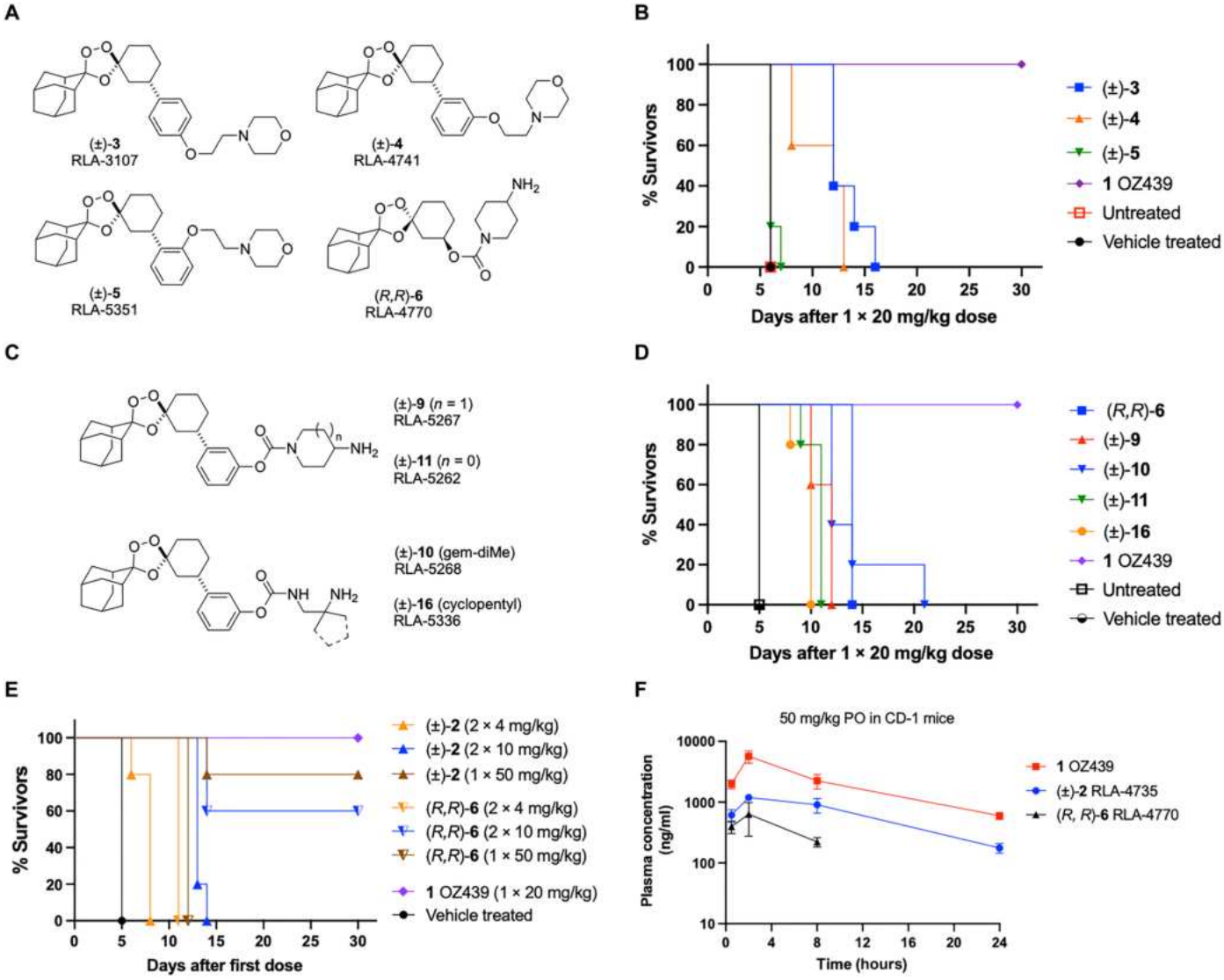

Fig. 3. In vivo efficacy and PK profiles of trans-3″ trioxolane analogs as compared to the cis-4″ comparator artefenomel (1, OZ439). (**A**) Structures of regioisomeric trans-3″-aryl trioxolane analogs **3** to **5** and the trans-3″-carbamate exemplar (*R*,*R*)-**6**. (**B**) Kaplan-Meier survival curves comparing the efficacy of **3** to **5** in the *P. berghei* mouse infection model following a single oral dose of 20 mg/kg. (**C**) Structures of selected trans-3″-aryl carbamate analogs **9** to **11** and **16**. (**D**) Kaplan-Meier survival curves showing efficacy of **6**, **9** to **11**, and **16** in the *P. berghei* model. (**E**) Kaplan-Meier curve for **1**, (±)-**2**, and **6** in the *P. berghei* mouse infection model when administered orally once daily at the indicated frequency and dose. (**F**) Plasma exposure curve for **1**, (±)-**2**, and (*R*,*R*)-**6** after a single oral (PO) dose of 50 mg/kg.

fresh clinical samples, which included K13 mutant parasites. With regard to their ADME properties, the HLM clearance values for both (*R*,*R*)-**2** and (*S*,*S*)-**2** were below the lower limit of the assay, while, unexpectedly, the enantiopure forms showed ~10-fold greater aqueous solubility than the racemate, all forms being evaluated as formate salts (Table 1). Last, both (*R*,*R*)-**2** and (*S*,*S*)-**2** exhibited fully curative efficacy (five of five mice) in the *P. berghei* model when administered as a single oral dose of 50 mg/kg (Fig. 4B). Thus, the in vitro ADME, in vitro antiplasmodial activity, and in vivo antimalarial efficacy were similar for enantiomeric forms of **2**.

Since it was not feasible to perform more extensive preclinical profiling with both enantiomeric forms of **2**, we arbitrarily selected (*S*,*S*)-**2** (RLA-5764) for further preclinical ADME and PK assessment (Table 3 and table S2). Thus, (*S*,*S*)-**2** showed excellent stability in human and mouse plasma as well as in microsomes and hepatocytes from rat, dog, and human [half-life ($t_{1/2}$) > 240 min in all assays]. Plasma protein binding was very high (>99.9%) across the three species and also very high in human hepatocytes and microsomes, mirroring the values reported for **1** (*46*). The blood to plasma ratio for (*S*,*S*)-**2** was 1.61 as compared to a value of 0.78 reported for **1.** Thermodynamic solubility (*S*,*S*)-**2** in fed-state simulated intestinal fluid was substantially higher (4525 μg/ml) than that in the fasted state (2.3 μg/ml). We determined permeability in Caco-2 monolayers using human plasma as the assay matrix, as has been recommended by Charman and colleagues (*47*) for compounds likely to have high membrane retention and low mass balance when using purely aqueous transport media. When corrected for free fraction using the human protein binding data, Caco-2 permeability for (*S*,*S*)-**2** was exceptionally high, with no evidence of active efflux. In summary, exemplar analog (*S*,*S*)-**2** exhibits high permeability, variable solubility

Table 1. Selected in vitro antiplasmodial activity and in vitro metabolism and solubility values for 1, 2 in racemic and single-enantiomer forms, regioisomeric 3″-aryl substituted congeners 3 to 5, and 3″-carbamate 6. IC_{50} values are average of three replicates ± SEM. Ranges reported when multiple measurements were performed. n.r., not reported; n.d., not determined.

	In vitro antiplasmodial or ADME assay data			
Compound	**W2 *P. falciparum* IC_{50} (nM)**	**HLM CL_{int} µl/min/mg**	**HLM $t_{1/2}$ (min)**	**Solubility PBS at pH 7.4 (µM)**
1	11 ± 0.5	72.1*	n.r.*	0.181*
(±)-**2**	6.1 ± 0.3	6.0†	229†	3.5–11.5
(±)-**3**	24 ± 0.6	21.6	65	24.8
(±)-**4**	29 ± 5.1	57.2	24	n.d.
(±)-**5**	53 ± 0.5	282	4.9	n.d.
(*R*,*R*)-**2**	3.8 ± 0.2	<11.6	>120	137–164
(*S*,*S*)-**2**	2.9 ± 0.2	<11.6	>120	78–80
(*R*,*R*)-**6**	1.7 ± 0.1‡	123†	11.3†	144.5†

*As reported by MMV (*46*). †Data generated via MMV. ‡From our previous report (*40*).

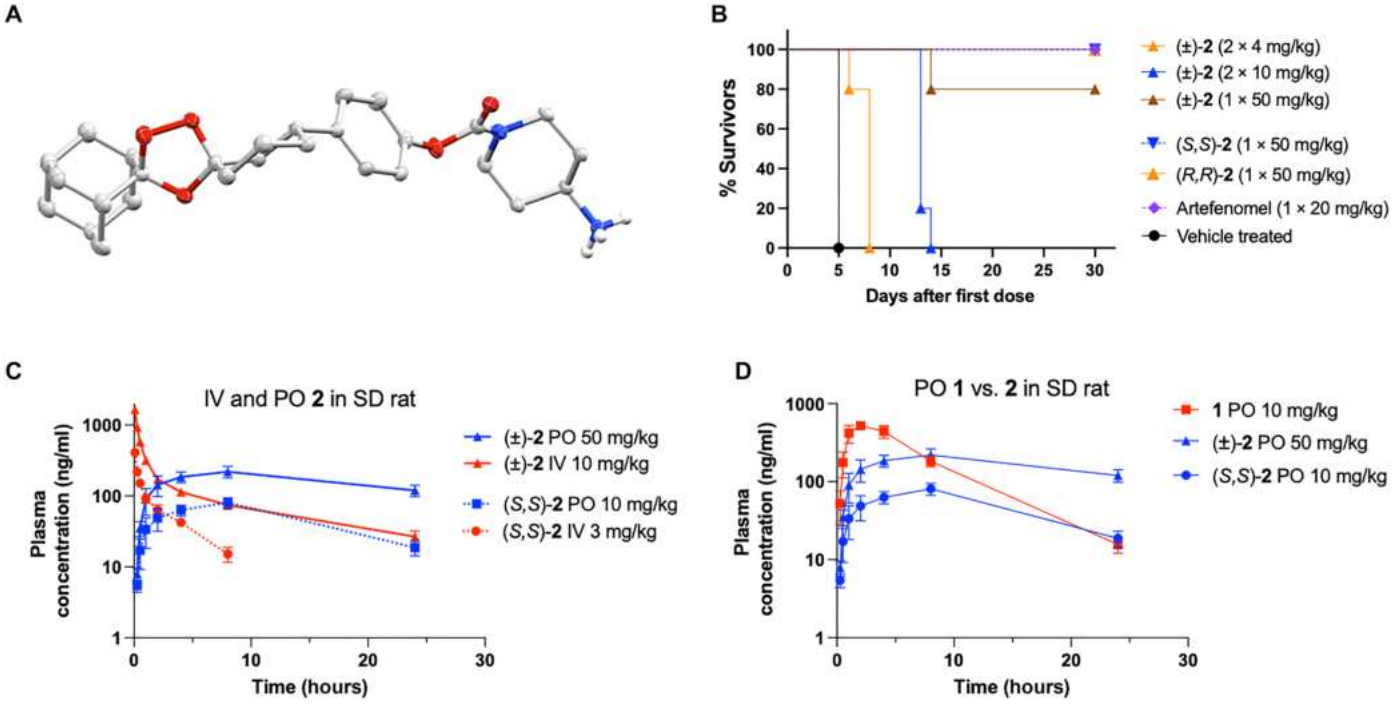

Fig. 4. Confirmation of absolute configuration of (*R*,*R*)-2 and in vivo PK/PD properties of 2 in racemic and enantiomerically pure forms. (**A**) Molecular structure of (*R*,*R*)-**2** from the crystal structure of the HCl salt (thermal ellipsoids drawn at the 30% probability level). Additional identical copies in the asymmetric unit, water molecules, chloride counterions, and carbon-bound hydrogens have been omitted for clarity. (**B**) Kaplan-Meier curves showing in vivo efficacy of (±)-**2**, (*S*,*S*)-**2**, and (*R*,*R*)-**2** in the *P. berghei* mouse malaria model at the indicated doses and dosing regimens. (**C**) PK profile of (±)-**2** and (*S*,*S*)-**2** in SD rat, following oral and intravenous (IV) doses of 50 and 10 mg/kg, and 10 and 3 mg/kg, respectively. (**D**) Comparison of plasma exposure in SD rat, following oral dose of **1**, (±)-**2**, or (*S*,*S*)-**2** at the indicated dose. PK data for **1** are from (*11*) and was provided by S. Charman (Monash Institutes of Pharmaceutical Sciences).

depending on the matrix, low clearance by microsomes and hepatocytes across preclinical and clinical species, and very high protein binding. Overall, the in vitro antiplasmodial potency, high predicted metabolic stability, and blood-plasma partitioning of (*S*,*S*)-**2** are all favorable for a potential TCP-1 class antimalarial.

Next, we studied (±)-**2** and (*S*,*S*)-**2** in mouse and rat PK studies following intravenous or oral administration. A PK study in mice administered (±)-**2** by the oral (50 mg/kg), and intravenous (10 mg/kg) routes revealed not only a very large volume of distribution (Vss = 22.7 liters/kg) but also unexpectedly high plasma clearance (CL = 147 ml/min per kilogram) considering the very low in vitro microsome and hepatocyte clearance values (fig. S11 and table S3). Exposure by the oral route was favorable with a $t_{1/2}$ of 7 hours and a mean residence time of 9.8 hours, suggesting that half-life is driven by Vss rather than CL (table S3). We next performed a PK study of (±)-**2** in Sprague-Dawley (SD) rat at the same oral and intravenous

Table 2. In vitro antiplasmodial activity of (*R*,*R*)-2, (*S*,*S*)-2, and DHA against laboratory-adapted Ugandan *P. falciparum* bearing K13 mutations and/or high RSAs against DHA. IC_{50} values ± SD with $N = 3$ except where SD is not reported. K13 genotypes at time of collection are indicated. Single-nucleotide polymorphisms were later confirmed for BUS-25 and PAT-26 strains.

Compound	PBC-403 K13 A578S	BUS-25 K13 C469Y	PAT-25 K13 C469Y	PAT-26 K13 C469Y	BUS-41 K13 WT
			IC_{50} (nM)		
(*R*,*R*)-**2**	2.78 ± 1.46	1.34 ± 0.55	1.90 ± 1.02	0.50 ± 0.18	0.73 ± 0.37
(*S*,*S*)-**2**	1.56 ± 0.84	0.16 ± 0.03	0.76 ± 0.23	0.50 ± 0.21	0.29 ± 0.07
DHA	1.49	3.88 ± 1.04	0.67	1.84 ± 0.48	0.57
			RSA (%)		
DHA	16.6	15.3	14.0	10.6	3.75

Table 3. Selected in vitro ADME properties determined for artefenomel (1), (±)-2, and (*S*,*S*)-2. Additional ADME assay data and values for all controls is provided in table S1.

ADME property*	1	(±)-2	(*S*,*S*)-2
HLM CLint, app (μl/min/mg protein)	63.7†	6.0†	<11.6
MLM CLint, app (μl/min/mg protein)	8.4†	14.1†	n.d.
Human plasma stability $t_{1/2}$ (min)	n.d.	n.d	>480
Mouse plasma stability $t_{1/2}$ (min)	n.d.	n.d.	251.4
PBS solubility at pH 7.4(μM)	0.181‡	11.5	79.7
Log*D* (octanol/PBS at pH 7.4) measured	5.81†	4.54†	n.d.
FaSSIF pH 6.5 (μg/ml)	40.6‡	n.d.	2.3
FeSSIF pH 5.0 (μg/ml)	536‡	n.d.	4525

*HLM and mouse liver microsome (MLM) intrinsic clearance, kinetic solubility in PBS at pH 7.4; thermodynamic solubility in fasted-state simulated intestinal fluid (FaSSIF) or fed-state simulated intestinal fluid (FeSSIF). †Values generated in head-to-head experiments contracted by MMV (project code CR302FB2). ‡Data from (*46*). Unless otherwise indicated, ADME data were determined by Quintara Biosciences (South San Francisco, CA).

doses of 50 and 10 mg/kg, respectively, and again observed both a high volume of distribution (Vss = 34.4 liters/kg), high clearance, and a long $t_{1/2}$ and mean residence time (MRT) of ~10 hours (Fig. 4C and table S4). To better compare with published blood clearance data for **1**, we evaluated (*S*,*S*)-**2** in SD rats at oral and intravenous doses of 10 and 3 mg/kg, respectively. The CL_{blood} value of 55.8 ml/min per kilogram and Vss_{blood} of 10.9 liter/kg for (*S*,*S*)-**2** lie between those reported for arterolane and **1** (Table 4 and table S5). Renal clearance of (*S*,*S*)-**2** was minimal, at 0.82 ml/min per kilogram (fraction in urine, <1%), ruling out renal extraction as a clearance mechanism (table S5). The oral bioavailability of (*S*,*S*)-**2** in rat was 76%, exactly the same value reported for **1** (Table 4), although different oral formulations were used. Comparing the rat plasma exposure curves for (*S*,*S*)-**2** with the historical data for **1** indicates higher exposure of **1** at the earlier time points but similar exposure for the two compounds by 24 hours (Fig. 4D). The favorable blood:plasma partitioning of (*S*,*S*)-**2**, combined with high volume of distribution and protein binding likely contribute to the extended exposure profile, despite high hepatic clearance. The higher plasma AUC of **1** in rodents also explains the compound's superior efficacy in the *P. berghei* mouse malaria model. Conversely, the enhanced stability of (*S*,*S*)-**2** in HLMs and hepatocytes predicts for an improved metabolic profile in humans.

Enhanced iron stability combined with half-life extension has been advanced as a criterion for addressing ART-R in next-generation endoperoxides (*4*, *30*). This same objected figured in the development of **1** (*37*), as the first-generation trioxolane arterolane had shown reduced exposure and serum half-life in infected patients compared to healthy volunteers (*48*, *49*). We therefore compared the intrinsic (cell-free) iron reactivity of **1** and (±)-**2** with that of the representative alkyl carbamate analog (*R*,*R*)-**6**. Consistent with expectations, aryl analogs **1** and (±)-**2** were markedly more stable (less reactive) toward ferrous iron than **6**, while (±)-**2** was the most stable, with >50% remaining for 24 hours after exposure to excess ferrous ammonium sulfate in an anoxic chamber (Table 5 and fig. S12).

To evaluate the effect of (±)-**2** in against clinically relevant parasites, we determined ex vivo RSAs for DHA, **1**, and (±)-**2** against parasites obtained from subjects with symptomatic *P. falciparum* infection in Uganda in 2019 and subsequently again in 2023–2024. In testing performed in 2019, the median IC_{50} values were 1.5 nM for DHA, 0.5 nM for **1**, and 2.6 nM for compound (±)-**2**, while RSA median survival was 0% for all three test compounds, consistent with a near absence of ART-R in this region in 2019 (Fig. 5, A and B). In the larger collection of isolates screened in 2023–2024, median IC_{50} values were 3.7 nM for DHA, 3.1 nM for **1**, and 3.8 nM for (±)-**2**, while RSA median survival rose substantially to 5.3% (range, 0.0 to 39.1%) for DHA but remained at 0.0% for **1** and 0.0% for (±)-**2** (Fig. 5, C and D, and table S6). The higher median RSA values for DHA in 2023–2024 as compared to 2019 are consistent with

Table 4. Comparison of selected PK parameters for arterolane and artefenomel compared to (*S*,*S*)-2 in male SD rats (*n* = 3 per group).

			Intravenous values (3 mg/kg)		Oral values (10 mg/kg)	
	Log $D_{7.4}$	B:P ratio	CL_{blood} (μl/min/kg)	Vss_{blood} (liter/kg)	$t_{1/2}$	*F* (%)
Arterolane (OZ277)	2.6*	1.5*	61	4.0	0.92	13
Artefenomel (**1**)	5.81	0.8*	33†	15†	24	76
(*S*,*S*)-**2**	4.54	1.6	55.8	10.9	9	76

*CL_{blood} and Vss_{blood} values are calculated from the plasma PK values and blood:plasma (B:P) ratios. Data for arterolane and artefenomel as reported (*11*). Arterolane measured Log*D* value as reported (*46*). †Intravenous dose for artefenomel was 2 mg/kg. For reference, liver blood flow (rat) = 68 ml/min per kilogram.

Table 5. Relative reactivity of artefenomel (1), (±)-2, and (*S*,*S*)-6 in 50 mM ferrous ammonium sulfate in citrate buffer under anaerobic conditions to minimize oxidation of the iron source by atmospheric oxygen.

	% Parent compound remaining at indicated time point			
Compound	**0 hours**	**2 hours**	**8 hours**	**24 hours**
1	100%	83%	54%	0%
(±)-**2**	100%	83%	79%	67%
(*S*,*S*)-**6**	100%	0%*	0%	0%

*(*S*,*S*)-**6** was fully consumed by 15 min.

emergence of ART-R over this time frame (*20*, *21*) and was confirmed by genotyping of the clinical samples (dataset S2). In summary, the data provided herein for trans-3″-aryl carbamate exemplar (±)-**2** revealed improved physiochemical properties compared to **1**, single-exposure efficacy in standard mouse models of malaria, enhanced iron stability and predicted metabolic stability in humans compared to **1**, and ex vivo RSAs superior to DHA in confirmed K13 mutant clinical strains.

DISCUSSION

The current study was motivated by the worrisome emergence of ART-R in malaria endemic regions and by the recent decision to halt further clinical evaluation of **1**. The remarkable efficacy of **1** in mouse malaria models and a keen desire for agents that achieve single-exposure cure led to its nomination as a development candidate. However, achieving single-dose efficacy clinically proved challenging, especially considering the high doses of **1** and the partner drug required, its poor stability in human microsomes, and formulation challenges. We hypothesized that the transverse molecular symmetry and amphiphilic nature of **1** likely contribute to its poor solubility and the formation (*45*) of micelles and lamellar phases in aqueous solution. By breaking symmetry with trans-3″ substitution as in exemplar **2**, we sought to both improve aqueous solubility while maintaining pharmacologically desirable rates of iron reactivity. Although we did observe notable improvements in aqueous solubility for **2** (in kinetic assays), further studies would be required to fully assess whether the compound or more optimized congeners share the complex solution-phase behavior of **1**.

The unusual pleiotropic-covalent pharmacology of endoperoxide-class antimalarial agents arguably requires design criteria distinct from those of traditional enzyme inhibitors. The "free drug hypothesis" posits that only unbound, free drug can exert a PD effect at its target, making the free fraction and unbound clearance important parameters for predicting efficacy and dose. However, for endoperoxide antimalarials, covalent cross-linking reactions to parasite proteins are responsible for the desired PD effect. Their binding affinity for parasite versus host proteins, kinetics of iron activation, and cross-linking profile will vary for different analogs, and how these various factors interact to determine efficacy is largely unknown. We hypothesize, however, that to address ART-R, a high degree of binding to parasite protein is almost certainly a favorable property, insofar as it helps stabilize and retain unreacted endoperoxide species through the transformation of resistant rings into more susceptible trophozoite and schizont parasite stages, where activating free heme iron is again abundant.

With these considerations in mind and guided by initial assessment for in vitro potency, solubility, and stability toward human microsomes and hepatocytes, we identified the favorable properties of trans-3″ trioxolane analogs bearing para-aryl carbamate side chains. Selecting from among the most promising analogs of this type, we studied the exemplar **2** in its racemic and enantiopure (*S*,*S*) form. In the *P. berghei* mouse malaria model, (*S*,*S*)-**2** afforded cures of all animals following a single oral dose of 50 mg/kg, despite having blood clearance near the rate of liver blood flow in the PD species. Other aspects of the PK profile of **2** were more favorable, including a high volume of distribution, extended in vivo half-life and mean residence time, and low renal clearance. Determining the root cause of the higher than predicted clearance in rodents would assist greatly in making more robust predictions of human dose and exposure and is a focus of current efforts.

In studies with cultured *P. falciparum*, (*S*,*S*)-**2** demonstrated potent low-nanomolar activity, with IC_{50} values similar to those of DHA and **1** against artemisinin-sensitive parasites and improved ex vivo RSA values to DHA against clinical strains of *P. falciparum*, including those with confirmed K13 mutations. These results offer promise for (*S*,*S*)-**2** and related, further optimized congeners to treat drug sensitive and ART-R falciparum malaria. Ideally, a next-generation trioxolane will produce cures in patients infected by artemisinin-sensitive or ART-R falciparum malaria, with reduced dosing frequencies, and will be readily coformulated with suitable partner drug. Considering this, the artefenomel-adjacent chemotype described herein, as exemplified by (*S*,*S*)-**2**, offers an important advance on the road to next-generation antimalarial combinations that provide reliable treatment of malaria in the setting of ART-R.

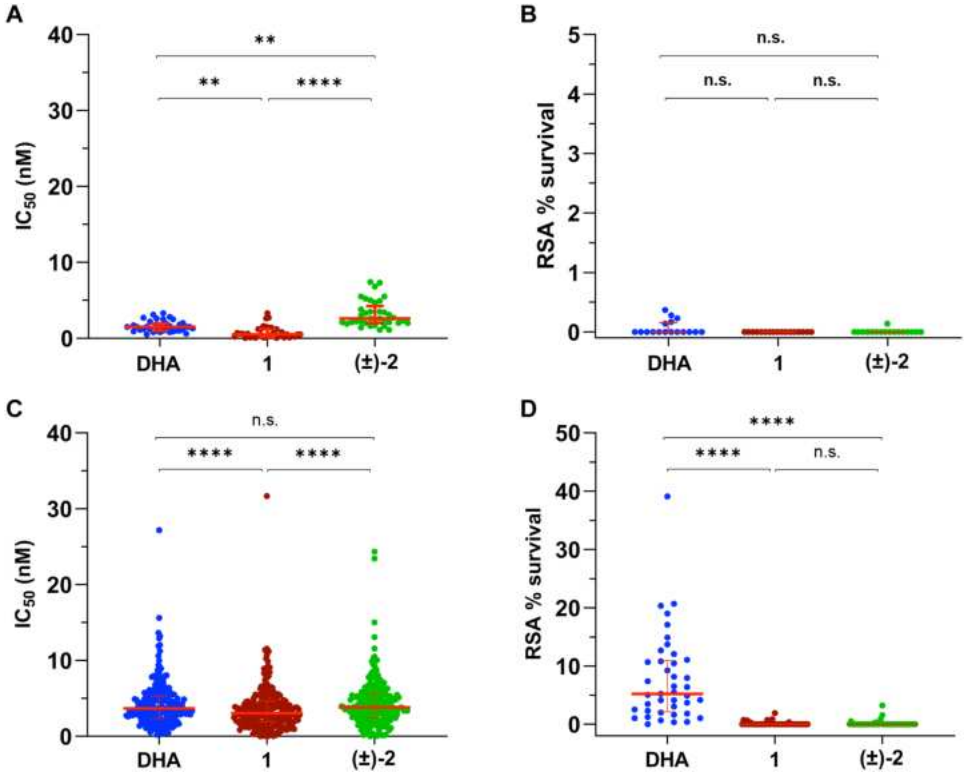

Fig. 5. Drug susceptibility of *P. falciparum* field isolates from Uganda. Drug susceptibility testing was performed in 2019 (**A** and **B**) and 2023–2024 (**C** and **D**) against DHA, artefenomel (**1**), and (±)-**2** measured as IC_{50} values in growth inhibition assay (A and C) and RSA survival rates (B and D) (note different scale on *y* axis). Multiple comparisons were made using the Friedman test for paired measures with Dunn's post hoc multiple comparison test (**$P < 0.01$; ****$P < 0.0001$). n.s., not significant.

MATERIALS AND METHODS

Additional Methods are found in the Supplementary Materials.

Materials

All chemical reagents were obtained commercially and used without further purification unless otherwise stated. Anhydrous solvents were purchased from Sigma-Aldrich and were used without further purification. Solvents used for flash column chromatography and work-up procedures were purchased form either Sigma-Aldrich or Thermo Fisher Scientific. Column chromatography was performed on SiliCycle SiliaPrep cartridges using a Biotage Isolera Four automated flash chromatography system. Compounds (±)-**3** (*41*) and (*R*,*R*)-**6** (*40*) were prepared as described previously by our group.

Ferrous iron stability studies of 1, (±)-2, and (*R*,*R*)-6

A 1 mM solution of test compound (prepared from 10 mM DMSO stock solution) was added to citrate buffer containing 50 mM $Fe(NH_4)_2(SO_4)_2{\cdot}6H_2O$ in an Ar(g)-purged glove bag to minimize oxidation of the ferrous iron salt. The solution was transferred to a heating block and warmed to 37°C. Aliquots (40 μl) of the reaction mixture were taken at four time points ($T = 15$ min and 2, 8, and 19 hours) and a 5-μl portion analyzed by ultraperformance liquid chromatography with ultraviolet (UV) detection at 190 nm to detect the ketone function shared by reaction products from all three test compounds. Quantification of reaction products was performed by integration of peaks for ketone intermediate in the UV chromatogram. Chromatograms were stacked and plotted in GraphPad Prism software.

P. berghei mouse malaria model

Female Swiss Webster mice (~20 g of body weight) were infected intraperitoneally with 10^6 *P. berghei*–infected erythrocytes collected from a previously infected mouse. Beginning 1 hour after inoculation, the mice were treated once daily by oral gavage for 1 or 2 days, as indicated with 100 μl of test compound solution formulated in 10% DMSO, 40% of a 20% 2-hydroxypropyl-β-cyclodextrin solution in water, and 50% PEG400. There were five mice in each test arm. Infections were monitored by daily microscopic evaluation of Giemsa-stained blood smears starting on day 7. Parasitemia was determined by counting the number of infected erythrocytes per 1000 erythrocytes. Body weight was measured over the course of the treatment. Mice were euthanized when parasitemia exceeded 50% or when weight loss of more than 15% occurred. Parasitemia, animal survival, and morbidity were closely monitored for 30 days postinfection, when experiments were terminated.

PK studies in mice

The mouse PK study of **1**, (±)-**2**, and (*R*,*R*)-**6** with oral dosing at 50 mg/kg (Fig. 2F) was performed in 8-week-old male CD-1 (ICR) mice (25 to 30 g, $n = 6$ per group) using a formulation of 10% DMSO, 40% of a 20% 2-hydroxypropyl-β-cyclodextrin solution in water, and 50% PEG400. Sampling was at 0.5, 2, 6, and 24 hours. Two blood samples (300 μl each) were collected from each mouse; three mice were assigned for each time point. The second/final blood collection was terminal. The plasma drug level data will be analyzed using Phoenix WinNonlin (version 6.3) software to perform non-compartmental modeling.

The mouse PK study of (±)-**2** with intravenous (10 mg/kg) and oral (50 mg/kg) dosing (Fig. 3C) was performed in male CD-1 (ICR) mice (18 to 22 g, $n = 3$ per group) with a formulation of 2% DMSO:98% of a 10.5% 2-hydroxypropyl-β-cyclodextrin solution in water. Microsampling (40 μl) via facial vein was performed at 0, 0.083, 0.25, 0.5, 1, 2, 4, 8, and 24 hours into K_2EDTA tubes. The blood samples were collected and centrifuged to obtain plasma (8000 rpm for 5 min) within 15 min postsampling. Nine blood samples were collected from each mouse; three samples were collected for each time point. Data were processed by Phoenix WinNonlin (version 8.3); samples below limit of quantitation were excluded in the PK parameters and mean concentration calculation.

PK studies in rat

The rat PK study of (±)-**2** with intravenous (10 mg/kg) and oral (50 mg/kg) dosing (Fig. 3D) was performed male SD rat (180 to 250 g, $n = 3$ per group) using a formulation of 2% DMSO:98% of a 10.5% 2-hydroxypropyl-β-cyclodextrin solution in water. Blood samples (100 μl) were collected via facial vein at 0, 0.083, 0.25, 0.5, 1, 2, 4, 8, and 24 hours into K_2EDTA tubes. The blood samples were collected and centrifuged to obtain plasma (8000 rpm for 5 min) within 15 min postsampling. Nine blood samples were collected from each mouse; three samples were collected for each time point. Data were processed by Phoenix WinNonlin (version 8.3); samples below limit of quantitation were excluded in the PK parameters and mean concentration calculation.

The rat PK study of (*S*,*S*)-**2** with intravenous (3 mg/kg) and oral (10 mg/kg) dosing (Fig. 3D) was performed male SD rat (220 to 250 g, $n = 3$ per group) using a formulation of 10% DMSO, 40% of a 20% 2-hydroxypropyl-β-cyclodextrin solution in water, and 50% PEG400. Blood samples (150 μl) were collected via jugular vein at 0, 0.083, 0.25, 0.5, 1, 2, 4, 8, and 24 hours into K_2EDTA tubes. The blood samples were collected and centrifuged to obtain plasma (2000*g* for 5 min) within 15 min postsampling. Nine blood samples were collected from each mouse; three samples were collected for each time point. Urine was collected at 0 to 4 hours, 4 to 8 hours, and 8 to 24 hours. Data were processed by Phoenix WinNonlin (version 8.2); samples below limit of quantitation were excluded in the PK parameters and mean concentration calculation.

Animal welfare

All animal use protocols were approved by the Institutional Animal Care and Use Committees (IACUC) at the University of California, San Francisco and were conducted in strict accordance with the National Institutes of Health Guide for the Care and Use of Laboratory Animals [National Research Council (US) Committee for the Update of the Guide for the Care and Use of Laboratory Animals, 2011]. The relevant IACUC approval number is AN203407 entitled "A murine model of malaria" and for rodent PK studies, AN194778, entitled "In vivo evaluation of experimental anti-cancer therapeutics; UCSF Preclinical Therapeutics Core." The mice were housed in a pathogen-free facility with controlled temperature and humidity, a 12-hour light/dark cycle, and ad libitum access to water and standard laboratory rodent chow.

Supplementary Materials

The PDF file includes:

Supplementary Text
Figs. S1 to S12
Tables S1 to S6
Legends for data S1 and S2
References

Other Supplementary Material for this manuscript includes the following:

Data S1 and S2

REFERENCES AND NOTES

1. *World Malaria Report 2023* (World Health Organization, 2023).
2. S. R. Meshnick, A. Thomas, A. Ranz, C. M. Xu, H. Z. Pan, Artemisinin (qinghaosu): The role of intracellular hemin in its mechanism of antimalarial action. *Mol. Biochem. Parasitol.* **49**, 181–189 (1991).
3. G. H. Posner, C. H. Oh, Regiospecifically oxygen-18 labeled 1,2,4-trioxane: A simple chemical model system to probe the mechanism(s) for the antimalarial activity of artemisinin (qinghaosu). *J. Am. Chem. Soc.* **114**, 8328–8329 (1992).
4. N. Klonis, D. J. Creek, L. Tilley, Iron and heme metabolism in *Plasmodium falciparum* and the mechanism of action of artemisinins. *Curr. Opin. Microbiol.* **16**, 722–727 (2013).
5. J. Wang, C.-J. Zhang, W. N. Chia, C. C. Y. Loh, Z. Li, Y. M. Lee, Y. He, L.-X. Yuan, T. K. Lim, M. Liu, C. X. Liew, Y. Q. Lee, J. Zhang, N. Lu, C. T. Lim, Z.-C. Hua, B. Liu, H.-M. Shen, K. S. W. Tan, Q. Lin, Haem-activated promiscuous targeting of artemisinin in *Plasmodium falciparum*. *Nat. Commun.* **6**, 10111 (2015).
6. H. M. Ismail, V. Barton, M. Phanchana, S. Charoensutthivarakul, M. H. L. Wong, J. Hemingway, G. A. Biagini, P. M. O'Neill, S. A. Ward, Artemisinin activity-based probes identify multiple molecular targets within the asexual stage of the malaria parasites *Plasmodium falciparum* 3D7. *Proc. Natl. Acad. Sci. U.S.A.* **113**, 2080–2085 (2016).
7. G. Siddiqui, C. Giannangelo, A. De Paoli, A. K. Schuh, K. C. Heimsch, D. Anderson, T. G. Brown, C. A. MacRaild, J. Wu, X. Wang, Y. Dong, J. L. Vennerstrom, K. Becker, D. J. Creek, Peroxide antimalarial drugs target redox homeostasis in *Plasmodium falciparum* infected red blood cells. *ACS Infect. Dis.* **8**, 210–226 (2022).
8. N. J. White, Assessment of the pharmacodynamic properties of antimalarial drugs in vivo. *Antimicrob. Agents Chemother.* **41**, 1413–1422 (1997).
9. C. W. Jefford, Synthetic peroxides as potent antimalarials. News and views. *Curr. Top. Med. Chem.* **12**, 373–399 (2012).
10. J. L. Vennerstrom, S. Arbe-Barnes, R. Brun, S. A. Charman, F. C. K. Chiu, J. Chollet, Y. Dong, A. Dorn, D. Hunziker, H. Matile, K. McIntosh, M. Padmanilayam, J. Santo Tomas, C. Scheurer, B. Scorneaux, Y. Tang, H. Urwyler, S. Wittlin, W. N. Charman, Identification of an antimalarial synthetic trioxolane drug development candidate. *Nature* **430**, 900–904 (2004).
11. S. A. Charman, S. Arbe-Barnes, I. C. Bathurst, R. Brun, M. Campbell, W. N. Charman, F. C. K. Chiu, J. Chollet, J. C. Craft, D. J. Creek, Y. Dong, H. Matile, M. Maurer, J. Morizzi, T. Nguyen, P. Papastogiannidis, C. Scheurer, D. M. Shackleford, K. Sriraghavan, L. Stingelin, Y. Tang, H. Urwyler, X. Wang, K. L. White, S. Wittlin, L. Zhou, J. L. Vennerstrom, Synthetic ozonide drug candidate OZ439 offers new hope for a single-dose cure of uncomplicated malaria. *Proc. Natl. Acad. Sci. U.S.A.* **108**, 4400–4405 (2011).
12. H. S. Kim, J. T. Hammill, R. K. Guy, Seeking the elusive long-acting ozonide: Discovery of artefenomel (OZ439). *J. Med. Chem.* **60**, 2651–2653 (2017).
13. The malERA Consultative Group on Drugs, A research agenda for malaria eradication: Drugs. *PLoS Med.* **8**, e1000402 (2011).
14. J. N. Burrows, R. H. van Huijsduijnen, J. J. Möhrle, C. Oeuvray, T. N. C. Wells, Designing the next generation of medicines for malaria control and eradication. *Malar. J.* **12**, 187 (2013).
15. N. J. White, F. H. Nosten, SERCAP: Is the perfect the enemy of the good? *Malar. J.* **20**, 281 (2021).
16. A. P. Phyo, P. Jittamala, F. H. Nosten, S. Pukrittayakamee, M. Imwong, N. J. White, S. Duparc, F. Macintyre, M. Baker, J. J. Möhrle, Antimalarial activity of artefenomel (OZ439), a novel synthetic antimalarial endoperoxide, in patients *with Plasmodium falciparum* and *Plasmodium vivax* malaria: An open-label phase 2 trial. *Lancet Infect. Dis.* **16**, 61–69 (2016).
17. F. Macintyre, Y. Adoke, A. B. Tiono, T. T. Duong, G. Mombo-Ngoma, M. Bouyou-Akotet, H. Tinto, Q. Bassat, S. Issifou, M. Adamy, H. Demarest, S. Duparc, D. Leroy, B. E. Laurijssens, S. Biguenet, A. Kibuuka, A. K. Tshefu, M. Smith, C. Foster, I. Leipoldt, P. G. Kremsner, B. Q. Phuc, A. Ouedraogo, M. Ramharter, OZ-Piperaquine Study Group, A randomised, double-blind clinical phase II trial of the efficacy, safety, tolerability and pharmacokinetics of a single dose combination treatment with artefenomel and piperaquine in adults and children with uncomplicated *Plasmodium falciparum* malaria. *BMC Med.* **15**, 181 (2017).
18. Y. Adoke, R. Zoleko-Manego, S. Ouoba, A. B. Tiono, G. Kaguthi, J. E. Bonzela, T. T. Duong, A. Nahum, M. Bouyou-Akotet, B. Ogutu, A. Ouedraogo, F. Macintyre, A. Jessel, B. Laurijssens, M. H. Cherkaoui-Rbati, C. Cantalloube, A. C. Marrast, R. Bejuit, D. White, T. N. C. Wells, F. Wartha, D. Leroy, A. Kibuuka, G. Mombo-Ngoma, D. Ouattara, I. Mugenya, B. Q. Phuc, F. Bohissou, D. P. Mawili-Mboumba, F. Olewe, I. Soulama, H. Tinto, FALCI Study Group, A randomized, double-blind, phase 2b study to investigate the efficacy, safety, tolerability and pharmacokinetics of a single-dose regimen of ferroquine with artefenomel in adults and children with uncomplicated *Plasmodium falciparum* malaria. *Malar. J.* **20**, 222 (2021).
19. Y. He, S. Campino, E. Diez Benavente, D. C. Warhurst, K. B. Beshir, I. Lubis, A. R. Gomes, J. Feng, W. Jiazhi, X. Sun, F. Huang, L.-H. Tang, C. J. Sutherland, T. G. Clark, Artemisinin resistance-associated markers in *Plasmodium falciparum* parasites from the China-

Myanmar border: Predicted structural stability of K13 propeller variants detected in a low-prevalence area. *PLOS ONE* **14**, e0213686 (2019).
20. M. D. Conrad, V. Asua, S. Garg, D. Giesbrecht, K. Niaré, S. Smith, J. F. Namuganga, T. Katairo, J. Legac, R. M. Crudale, P. K. Tumwebaze, S. L. Nsobya, R. A. Cooper, M. R. Kamya, G. Dorsey, J. A. Bailey, P. J. Rosenthal, Evolution of partial resistance to artemisinins in malaria parasites in uganda. *N. Engl. J. Med.* **389**, 722–732 (2023).
21. P. J. Rosenthal, V. Asua, M. D. Conrad, Emergence, transmission dynamics and mechanisms of artemisinin partial resistance in malaria parasites in Africa. *Nat. Rev. Microbiol.* **22**, 373–384 (2024).
22. M. D. Conrad, P. J. Rosenthal, Antimalarial drug resistance in Africa: The calm before the storm? *Lancet Infect. Dis.* **19**, e338–e351 (2019).
23. G. Siddiqui, A. Srivastava, A. S. Russell, D. J. Creek, Multi-omics based identification of specific biochemical changes associated with PfKelch13-mutant artemisinin-resistant *Plasmodium falciparum*. *J Infect Dis* **215**, 1435–1444 (2017).
24. J. Birnbaum, S. Scharf, S. Schmidt, E. Jonscher, W. A. M. Hoeijmakers, S. Flemming, C. G. Toenhake, M. Schmitt, R. Sabitzki, B. Bergmann, U. Fröhlke, P. Mesén-Ramírez, A. Blancke Soares, H. Herrmann, R. Bártfai, T. Spielmann, A Kelch13-defined endocytosis pathway mediates artemisinin resistance in malaria parasites. *Science* **367**, 51–59 (2020).
25. H. M. Behrens, S. Schmidt, T. Spielmann, The newly discovered role of endocytosis in artemisinin resistance. *Med. Res. Rev.* **41**, 2998–3022 (2021).
26. N. F. Gnädig, B. H. Stokes, R. L. Edwards, G. F. Kalantarov, K. C. Heimsch, M. Kuderjavy, A. Crane, M. C. S. Lee, J. Straimer, K. Becker, I. N. Trakht, A. R. Odom John, S. Mok, D. A. Fidock, Insights into the intracellular localization, protein associations and artemisinin resistance properties of *Plasmodium falciparum* K13. *PLoS Pathog.* **16**, e1008482 (2020).
27. N. Klonis, M. P. Crespo-Ortiz, I. Bottova, N. Abu-Bakar, S. Kenny, P. J. Rosenthal, L. Tilley, Artemisinin activity against *Plasmodium falciparum* requires hemoglobin uptake and digestion. *Proc. Natl. Acad. Sci. U.S.A.* **108**, 11405–11410 (2011).
28. S. C. Xie, C. Dogovski, E. Hanssen, F. Chiu, T. Yang, M. P. Crespo, C. Stafford, S. Batinovic, S. Teguh, S. Charman, N. Klonis, L. Tilley, Haemoglobin degradation underpins the sensitivity of early ring stage *Plasmodium falciparum* to artemisinins. *J. Cell Sci.* **129**, 406–416 (2016).
29. B. Witkowski, D. Menard, C. Amaratunga, R. M. Fairhurst, "Ring-stage survival assays (RSA) to evaluate the in-vitro and ex-vivo susceptibility of *Plasmodium falciparum* to artemisinins" (Institute Pasteur du Cambodge–National Institutes of Health Procedure RSAv1, 2013), pp. 1–16.
30. T. Yang, S. C. Xie, P. Cao, C. Giannangelo, J. McCaw, D. J. Creek, S. A. Charman, N. Klonis, L. Tilley, Comparison of the exposure time dependence of the activities of synthetic ozonide antimalarials and dihydroartemisinin against K13 wild-type and mutant *Plasmodium falciparum* strains. *Antimicrob. Agents Chemother.* **60**, 4501–4510 (2016).
31. J. Straimer, N. F. Gnädig, B. H. Stokes, M. Ehrenberger, A. A. Crane, D. A. Fidock, *Plasmodium falciparum* K13 mutations differentially impact ozonide susceptibility and parasite fitness in vitro. *MBio* **8**, e00172-17 (2017).
32. C. Giannangelo, L. Stingelin, T. Yang, L. Tilley, S. A. Charman, D. J. Creek, Parasite-mediated degradation of synthetic ozonide antimalarials impacts in vitro antimalarial activity. *Antimicrob. Agents Chemother.* **62**, e01566-17 (2018).
33. P. M. O'Neill, G. H. Posner, A medicinal chemistry perspective on artemisinin and related endoperoxides. *J. Med. Chem.* **47**, 2945–2964 (2004).
34. Y. Dong, J. Chollet, H. Matile, S. A. Charman, F. C. K. Chiu, W. N. Charman, B. Scorneaux, H. Urwyler, J. Santo Tomas, C. Scheurer, C. Snyder, A. Dorn, X. Wang, J. M. Karle, Y. Tang, S. Wittlin, R. Brun, J. L. Vennerstrom, Spiro and dispiro-1,2,4-trioxolanes as antimalarial peroxides: Charting a workable structure-activity relationship using simple prototypes. *J. Med. Chem.* **48**, 4953–4961 (2005).
35. H. M. Ismail, V. E. Barton, M. Panchana, S. Charoensutthivarakul, G. A. Biagini, S. A. Ward, P. M. O'Neill, A click chemistry-based proteomic approach reveals that 1,2,4-trioxolane and artemisinin antimalarials share a common protein alkylation profile. *Angew. Chem. Int. Ed.* **55**, 6401–6405 (2016).
36. D. J. Creek, W. N. Charman, F. C. K. Chiu, R. J. Prankerd, K. J. McCullough, Y. Dong, J. L. Vennerstrom, S. A. Charman, Iron-mediated degradation kinetics of substituted dispiro-1,2,4-trioxolane antimalarials. *J. Pharm. Sci.* **96**, 2945–2956 (2007).
37. Y. Dong, X. Wang, S. Kamaraj, V. J. Bulbule, F. C. K. Chiu, J. Chollet, M. Dhanasekaran, C. D. Hein, P. Papastogiannidis, J. Morizzi, D. M. Shackleford, H. Barker, E. Ryan, C. Scheurer, Y. Tang, Q. Zhao, L. Zhou, K. L. White, H. Urwyler, W. N. Charman, H. Matile, S. Wittlin, S. A. Charman, J. L. Vennerstrom, Structure-activity relationship of the antimalarial ozonide artefenomel (OZ439). *J. Med. Chem.* **60**, 2654–2668 (2017).
38. S. D. Fontaine, A. G. DiPasquale, A. R. Renslo, Efficient and stereocontrolled synthesis of 1,2,4-trioxolanes useful for ferrous iron-dependent drug delivery. *Org. Lett.* **16**, 5776–5779 (2014).
39. B. R. Blank, J. Gut, P. J. Rosenthal, A. R. Renslo, Enantioselective synthesis and in vivo evaluation of regioisomeric analogues of the antimalarial arterolane. *J. Med. Chem.* **60**, 6400–6407 (2017).
40. B. R. Blank, R. L. Gonciarz, P. Talukder, J. Gut, J. Legac, P. J. Rosenthal, A. R. Renslo, Antimalarial trioxolanes with superior drug-like properties and in vivo efficacy. *ACS Infect. Dis.* **6**, 1827–1835 (2020).
41. B. R. Blank, J. Gut, P. J. Rosenthal, A. R. Renslo, Artefenomel regioisomer RLA-3107 is a promising lead for the discovery of next-generation endoperoxide antimalarials. *ACS Med. Chem. Lett.* **14**, 493–498 (2023).
42. J. N. Burrows, S. Duparc, W. E. Gutteridge, R. Hooft van Huijsduijnen, W. Kaszubska, F. Macintyre, S. Mazzuri, J. J. Möhrle, T. N. C. Wells, New developments in anti-malarial target candidate and product profiles. *Malar. J.* **16**, 26 (2017).
43. Y. Tang, Y. Dong, J. M. Karle, C. A. DiTusa, J. L. Vennerstrom, Synthesis of tetrasubstituted ozonides by the Griesbaum coozonolysis reaction: Diastereoselectivity and functional group transformations by post-ozonolysis reactions. *J. Org. Chem.* **69**, 6470–6473 (2004).
44. M. Salim, J. Khan, G. Ramirez, A. J. Clulow, A. Hawley, H. Ramachandruni, B. J. Boyd, Interactions of artefenomel (OZ439) with milk during digestion: Insights into digestion-driven solubilization and polymorphic transformations. *Mol. Pharm.* **15**, 3535–3544 (2018).
45. A. J. Clulow, M. Salim, A. Hawley, E. P. Gilbert, B. J. Boyd, The curious case of the OZ439 mesylate salt: An amphiphilic antimalarial drug with diverse solution and solid state structures. *Mol. Pharm.* **15**, 2027–2035 (2018).
46. S. A. Charman, A. Andreu, H. Barker, S. Blundell, A. Campbell, M. Campbell, G. Chen, F. C. K. Chiu, E. Crighton, K. Katneni, J. Morizzi, R. Patil, T. Pham, E. Ryan, J. Saunders, D. M. Shackleford, K. L. White, L. Almond, M. Dickins, D. A. Smith, J. J. Moehrle, J. N. Burrows, N. Abla, An in vitro toolbox to accelerate anti-malarial drug discovery and development. *Malar. J.* **19**, 1 (2020).
47. K. Katneni, T. Pham, J. Saunders, G. Chen, R. Patil, K. L. White, N. Abla, F. C. K. Chiu, D. M. Shackleford, S. A. Charman, Using human plasma as an assay medium in Caco-2 studies improves mass balance for lipophilic compounds. *Pharm. Res.* **35**, 210 (2018).
48. N. Valecha, S. Looareesuwan, A. Martensson, S. M. Abdulla, S. Krudsood, N. Tangpukdee, S. Mohanty, S. K. Mishra, P. K. Tyagi, S. K. Sharma, J. Moehrle, A. Gautam, A. Roy, J. K. Paliwal, M. Kothari, N. Saha, A. P. Dash, A. Björkman, Arterolane, a new synthetic trioxolane for treatment of uncomplicated *Plasmodium falciparum* malaria: A phase II, multicenter, randomized, dose-finding clinical trial. *Clin. Infect. Dis.* **51**, 684–691 (2010).
49. N. Valecha, D. Savargaonkar, B. Srivastava, B. H. K. Rao, S. K. Tripathi, N. Gogtay, S. K. Kochar, N. B. V. Kumar, G. C. Rajadhyaksha, J. D. Lakhani, B. B. Solanki, R. K. Jalali, S. Arora, A. Roy, N. Saha, S. S. Iyer, P. Sharma, A. R. Anvikar, Comparison of the safety and efficacy of fixed-dose combination of arterolane maleate and piperaquine phosphate with chloroquine in acute, uncomplicated *Plasmodium vivax* malaria: A phase III, multicentric, open-label study. *Malar. J.* **15**, 42 (2016).
50. C. M. Woodley, G. L. Nixon, N. Basilico, S. Parapini, W. D. Hong, S. A. Ward, G. A. Biagini, S. C. Leung, D. Taramelli, K. Onuma, T. Hasebe, P. M. O'Neill, Enantioselective synthesis and profiling of potent, nonlinear analogues of antimalarial tetraoxanes E209 and N205. *ACS Med. Chem. Lett.* **12**, 1077–1085 (2021).

Acknowledgments: This work is dedicated to the memory of our collaborator and colleague, Roland A. Cooper. We thank S. Charman and D. Creek (Monash Institutes of Pharmaceutical Sciences) for discussions and S. Charman for reviewing the manuscript. We thank R. Christofferson (Louisiana State University) and M. Conrad (UCSF) for help with statistical analyses and for compiling genotype data for the ex vivo strains, respectively. Selected in vitro ADME assay data (Table 2) were generated by CROs under contract to MMV (project code CR203FB2). All remaining ADME assay data were performed by Quintara Biosciences (South San Francisco, CA). PK study in CD-1 mice was performed by SRI Biosciences under contract with NIAID Preclinical Services (DMID contract no. HHSN272201100022I). PK studies of (±)-**2** in CD-1 mice and SD rat were performed by Tatara Therapeutics (San Francisco, CA). PK studies of (*S,S*)-**2** in SD rat were performed by Chempartner Corporation (South San Francisco, CA). **Funding:** This work was supported by NIH/NIAID grants AI075045 and AI139179 to P.J.R. and AI105106 and CA260860 to A.R.R. **Author contributions:** Conceptualization and research design: M.T.K., P.T., B.R.B., J.A.T., J.N.B., P.J.R., R.A.C., and A.R.R. Data collection and analysis: M.T.K., P.T., B.R.B., S.C., J.C., R.L.G., P.J., J.L., V.M., A.N., M.O., S.O., N.S.S., J.A.T., Y.T., P.K.T., and A.V. PK experiments and analysis: S.D.F. and G.J.L. Writing—original draft: M.T.K. and A.R.R. Review and edit: All authors. **Competing statement:** A.R.R. is a cofounder and holds equity in Tatara Therapeutics Inc., San Francisco, CA. S.D.F. and G.J.L. are employees of and hold equity in Tatara Therapeutics Inc., San Francisco, CA. A.R.R., P.T., and B.R.B. are listed as co-inventors on US patent no. 12,139,470 B2 (12 November 2024) entitled "Trioxolane agents" and associated published applications filed by The Regents of the University of California and Licensed to Tatara Therapeutics, Inc., San Francisco, CA. All other authors declare that they have no competing interests. **Data and materials availability:** All data needed to evaluate the conclusions in the paper are present in the paper and/or the Supplementary Materials. A crystallographic dataset is available as a separate file associated with this manuscript as data S1.

Submitted 3 September 2024
Accepted 8 July 2025
Published 8 August 2025
10.1126/sciadv.ads9168